Journal of Environmental Chemical Engineering 12 (2024) 111820

Contents lists available at ScienceDirect

Journal of Environmental Chemical Engineering

journal homepage: www.elsevier.com/locate/jece

Structured organic frameworks as endocrine disruptor adsorbents suitable for Fenton regeneration and reuse

Aida M. Díez [a,b,*], Juanjo García-Ocampo [a,b], Marta Pazos [b], M. Ángeles Sanromán [b], Yury V. Kolenko [a]

[a] Nanochemistry Research Group, International Iberian Nanotechnology Laboratory (INL), Braga 4715–330, Portugal
[b] CINTECX, Universidade de Vigo, BIOSUV group, Department of Chemical Engineering, 36310 Vigo, Spain

ARTICLE INFO

Keywords:
Adsorption process
Covalent organic frameworks
Desorption
Metal organic frameworks
Water pollution
Real wastewater treatment

ABSTRACT

New porous materials, such as metal-organic frameworks (MOFs) and covalent-organic frameworks (COFs), have been actively investigated due to their environmental applications. In this study, four of such structured materials, namely Fe_3O_4 @COF, MIL-53(Al), MIL-53(Al)-F127 and NH_2-MIL-101(Fe) were synthetized. These materials have been tested for the first time for the adsorption in aqueous media of two endocrine disruptor pollutants, bisphenol A (BPA) and prednisolone (PDN). The adsorbents were characterized by the analysis of the point of zero charge (PZC), the functional groups (FTIR) and their physic-chemical structure (N_2-isotherms, SEM, XRD and XPS). MIL-53-Al provided the highest uptake of both BPA (177.78 mg g^{-1}) and PDN (280.70 mg g^{-1}) even when using a real wastewater matrix. Additionally, this MOF resulted to be a so-called catalytic-adsorbent, maintaining an appropriate adsorbent capacity after five regenerations cycles via Fenton-like process, causing only 20% and 5% adsorption detriment for BPA and PDN, respectively. This avoids spent adsorbent disposal issues and make this new kind of adsorbent to have the potential to be used in real environmental application scenarios.

1. Introduction

The growth of world population and an intensive industrialization have created several environmental problems. For instance, water resources have been exposed to endocrine disruptor chemicals (EDCs) such as some pharmaceutical and personal care products, dyes, pesticides, industrial additives, etc [1,2]. Within EDCs, bisphenol A (BPA) is largely produced and has many industrial applications [3]. Unfortunately, BPA is an environmental threat because of its estrogenic effects and potential DNA damage [4]. Prednisolone (PDN) is a corticoid pharmaceutical which long exposure can cause mental disorders [5,6]. Besides, both BPA and PDN high stability is likely to cause their accumulation on the environment [3,5].

In recent years, the research on metal-organic frameworks (MOFs) and covalent-organic frameworks (COFs) has increased exponentially (Fig. S1 in the Supplementary Material) [7]. MOFs are hybrid crystalline porous materials formed by a metal cluster and organic linkers. COFs are built from organic monomers that are linked together by stable covalent bonds [8]. Both structured materials exhibit good chemical and thermal stability [9], as well as a high specific surface area, with multiple active sites available for adsorption and catalysis [10]. Overall, they present several advantages versus traditional adsorbents, such as their tunability, high surface area and catalytic properties, making them attractive for adsorption and catalysis processes [11,12].

There are few studies focused on the utilization of MOFs and COFs for the elimination of EDCs. Indeed, PDN adsorption has received limited attention in previous studies, and if investigated, it has been primarily conducted using conventional adsorbents rather than MOFs or COFs [13,14]. On the other hand, BPA has been adsorbed into MOFs [13–17], although their adsorption performance and subsequent regeneration should be improved to make this process feasible for future usages.

Unfortunately, landfilling is the main selected alternative for spent (polluted-containing) adsorbent disposal, risking future contamination of the surrounding environment as pollutants may leach from the spent adsorbents [18]. Alternatively, several interesting regeneration routes can be coupled to the adsorption process. Interestingly, applying directly the regeneration process to the spent adsorbent is an option to avoid

* Corresponding author at: CINTECX, Universidade de Vigo, BIOSUV group, Department of Chemical Engineering, 36310 Vigo, Spain.
E-mail address: adiez@uvigo.gal (A.M. Díez).

https://doi.org/10.1016/j.jece.2023.111820
Received 2 November 2023; Received in revised form 19 December 2023; Accepted 23 December 2023
Available online 2 January 2024

additional treatment steps, like the desorption and the further degradation of the polluted solution [19]. This direct regeneration adds a remarkable value to this research, considering the limited number of publications that include recovering technologies for the used adsorbents. For the first time, the regeneration of spent EDCs-containing COF and MOFs have been carried out.

Among the methods for the direct regeneration of the spent materials, advanced oxidation processes (AOPs) show huge potential due to their high pollutant degradation efficiency in water [20–22]. Typically, AOPs rely on the generation of hydroxyl radicals (•OH), species with a high oxidation potential between 2.8 V (pH = 0) and 1.95 V (pH = 14) [23]. Some methods for •OH generation are the application of ultrasounds, UV radiation, temperature or the addition of H_2O_2 with transition metal cations (M^n), on the so-called Fenton process (Eq. (1)) [24]. The disadvantage of this process is the associated pollution or recovery steps of the spent metal (M^{n+1}), and for that, the usage of the transition metal trapped in a matrix (heterogeneous catalyst) is investigated using the so-called Fenton-like process [20,25]. Moreover, AOPs are more suitable for high pollutant concentrations [25,26], and consequently, coupling AOPs to a pre-concentrated solution/adsorbent could be a feasible alternative. Indeed, some studies have tried to apply Fenton-based processes for polluted adsorbents' regeneration although more research should be done in order to increase pollutant uptake [27] or regeneration capacity [14].

$$H_2O_2 + M^{n+} \rightarrow \bullet OH + HO^- + M^{n+1} \quad (1)$$

In this study, we select and synthesize several previously reported framework compounds, based on MIL-type MOFs and a Fe_3O_4-containing-COF, considering the metal content within these materials could promote catalytic activity. Further, we, for the first time, investigate the applicability of the prepared and well-characterized materials for the dual adsorption of PDN and BPA pollutants while simultaneously addressing previously unreported direct regeneration by means of the Fenton-like process. Finally, the best performing framework material was employed during adsorption and regeneration cycles, as well as for the treatment of real wastewaters.

2. Materials and methods

2.1. Reagents

2.1.1. Target pollutants

Experiments were carried out using BPA (>99.0%) and PDN (>99.0%) as target pollutants, both purchased from Sigma-Aldrich. In addition, acetonitrile (99.9%, HPLC grade) from Fischer Scientific was used for BPA and PDN solutions preparation. This organic solvent (5%) was added to increase the solubility of the pollutants in water, and no adsorption differences were found vs. 100% water.

2.1.2. Reagents for the synthesis of the frameworks materials

Melamine (MA, $C_3H_6N_6$, 99%) and iron (III) chloride hexahydrate ($FeCl_3$•6 H_2O, ≥98.0%) were purchased from Acros Organics. Iron (II) chloride ($FeCl_2$, 97.0%) and iron (III) chloride ($FeCl_3$, 97.0%) from PanReac AppliChem, ITW reagents. Pluronic (F127) was acquired from Merk. Sodium hydroxide (NaOH≥98.0%), iron (III) chloride hexahydrate ($FeCl_3$·6 H_2O≥98.0%), dimethyl sulfoxide (DMSO≥99.5%), ethylene glycol ($C_2H_6O_2$, ≥99.8%), methanol (CH_3OH, ≥99.8%), tetrahydrofuran (C_4H_8O≥99.0%) dichloromethane (CH_2Cl_2 ≥99.8%) and 2-aminoterephtalic acid (NH_2-BCD, $C_8H_7NO_4$ 99.0%) were purchased from Sigma-Aldrich. Terephtaldehyde ($C_8H_6O_2$ ≥98.0%) and terephthalic acid ($C_8H_6O_4$ >99.0%) were obtained from TCI Chemicals.

2.1.3. Reagents for the regeneration of spent frameworks materials

H_2O_2 (30%) and acetonitrile (HPLC grade) were purchased from Sigma Aldrich. Ammonium chloride (NH_4Cl, 99.5%) was acquired from PanReac.

2.2. Synthesis of frameworks materials

2.2.1. Fe_3O_4 @COF

Fe_3O_4 nanoparticles were prepared based on our previous procedure [28]. Briefly, $FeCl_2$ and $FeCl_3$ were mixed, keeping 1:1.5 molar ratio. The solution was kept at 70ºC while 100 mL of NaOH 5 M were added dropwise using a peristaltic pump (Masterflex). The solution color changed from orange to brown, due to the formation of the magnetite nanoparticles. They were separated by vacuum filtration and washed several times with distilled water. Then, they were dried at 60ºC overnight.

Later, You et al. [29] procedure was adapted for the synthesis of the COF. From the Fe_3O_4 nanoparticles previously obtained, 0.2 g were dispersed in 40 mL of DMSO, containing MA (0.25 g) and TPA (0.2 g). The mixture was immersed in an ultrasonic bath for 30 min to get a proper dispersion and. Then, it was transferred to an autoclave and treated at 180 ºC for 24 h. Then, the product was recovered by vacuum filtration and washed with methanol, dichloromethane and tetrahydrofuran. Finally, the solid was vacuum-dried at 50 ºC overnight.

2.2.2. MIL-53(Al) and MIL-53(Al)-F127 MOFs

For MIL-53(Al) preparation, $Al(NO_3)_3$•9 H_2O (0.84 g) and H_2BDC (0.24 g) were added to a solution of DMF (11 mL) and water (4 mL). Next, the resultant mixture was transferred to an autoclave and treated for 48 h at 130 ºC. The product of the solvothermal synthesis was vacuum-filtered and washed several times with deionized water. To eliminate residual H_2BDC, the solid was submerged in a DMF solution for another 24 h. Finally, the attained white powder was vacuum-filtered again and dried for 12 h at 150 ºC.

For the synthesis of MIL-53(Al)-F127, 1.85 g of $Al(NO_3)_3$•9 H_2O and 0.46 g of H_2BDC were added to a solution formed by DMF (24.19 mL), water (9.11 mL) and ethanol (6.7 mL). Then, F127 (6.21 g) was slowly added under stirring and, after that, the mixture was kept under stirring for 2 additional h. Next, it was transferred to an autoclave and treated for 48 h at 130ºC. The product was recovered by vacuum filtration, and it was washed with water and ethanol. To eliminate unreacted F127, the solid was submerged in ethanol and the solution was kept under reflux at 70ºC for 48 h. Then, H_2BDC was eliminated by submerging the material into DMF for 24 h, whereupon it was filtered and finally dried at 150ºC for 12 h [30].

2.2.3. NH_2-MIL-101(Fe)

$FeCl_3$•6 H_2O (1.77 g) and NH_2-BCD (0.60 g) were added to DMF (40 mL) and the solution was immersed in an ultrasonic bath for 26 min, favouring particles dispersion. After sonication, it was transferred to an autoclave and treated for 20 h at 110ºC. The obtained product was washed several times with water, ethanol and DMF and, finally, it was dried at 60ºC overnight [31].

2.3. Pollutants quantification

To determine the pollutant removal capacities of the studied materials, high-performance liquid chromatography (HPLC) coupled to a diode array detector (DAD) was used, considering the typical spectra of BPA and PDN (Fig. S2). Samples were taken along each assay and filter (0.45 μm) prior to analysis. For that, the HPLC Agilent 1290 Infinity II equipped with the apolar column Kinetex 2.6 mm EVO C18 100 Å was used. 10 μL were injected and a gradient acetonitrile/water was used (Table S1), in which every sample is eluted for 18 min. The flow rate was 0.5 mL min^{-1} during the initial 10 min and then it was increased to 1 mL min^{-1} as well as the acetonitrile concentration, to avoid PDN or BPA accumulation on the column.

2.4. Water treatment experiments

2.4.1. Adsorption

In preliminary tests the adsorption capacity was compared for all the synthesized structured materials. Thus, 100 mL of a 100 mg/L BPA or PDN solution was mixed in a flask with 35 mg of the framework material. Flasks were stirred at 150 rpm in an orbital shaker (Thermo Scientific PRECISION SBW 27) at room temperature for 90 min. Some experiences were done in triplicate, obtaining a deviation under 4.1%. The adsorption capacity of the materials was evaluated by taking liquid test samples at the beginning and the end of the adsorption experiments, and the concentration was measured by HPLC.

2.4.2. Desorption

I order to quantify the regeneration process, the remaining pollutant was desorbed by a mixture 20/80 water/acetonitrile with NH_4Cl 0.2 M [32]. For that, 35 mg of saturated adsorbent were put into 35 mL of that desorption mixture Triplicate tests were done for the desorption of the saturated adsorbents, attaining a deviation below 3.9%.

2.4.3. Regeneration

To evaluate the potential of the synthesized framework adsorbents to be used as the catalysts for their regeneration purpose, Fenton-like process was carried out, assuming that the metals present in all the framework materials could act as catalytically active sites [32]. Moreover, oxidation via H_2O_2 addition is a common technique for the degradation of pollutants, (i.e. regenerating the adsorbent). This is due to the high oxidation potential of the •OH that are generated because of the reactions between pollutant and H_2O_2. This methodology has been successfully used for adsorbent regeneration in a number of studies [33,34].

Our regeneration testing was adapted from that of Taha and coworkers [35]. Briefly, 50 mg of pollutant-containing adsorbent were introduced in 50 mL of water, adding 88 mmol H_2O_2. The solution was stirred at room temperature for 2 h and, then, 10 μL of methanol were added to the system to quench the Fenton-like reaction [36].

2.5. Characterization

To achieve a comprehensive characterization of the catalytic adsorbents, various analytical techniques were applied. Physical characterization involved surface area analysis (N_2 isotherms), X-Ray diffraction (XRD), and scanning electron microscopy (SEM). For chemical characterization, experiments included Fourier-transform infrared spectroscopy (FTIR), X-Ray photoelectron spectroscopy (XPS), point of zero charge (PZC) determination, and electrochemical analyses of the materials.

2.5.1. N_2 isotherms

Surface analysis was done using, approximately, 100 mg of sample, which were placed into a tube holder. After that, they were put into the Autorosorb iQ_2 analyzer (Quantachrome, Boynton Beach, FL, USA) for the measurement. First, samples were degassed at 120 ºC for 180 min to eliminate possible dirtiness on the solids. Then, the sample holder containing the structured material was placed into a liquid nitrogen bath (at 77.53 K). The specific surface area was determined using Brunauer-Emmett-Teller (BET) method, that establishes a relation between gas amount adsorbed by an adsorbent and its surface area [37]. Total pore volume is calculated using the amount of vapor adsorbed at $P/P_0 \approx 1$, assuming the pores are filled with liquid adsorbate, so it is possible to convert adsorbed volume into liquid nitrogen volume. Finally, Barret-Joyner-Halenda (BHJ) method was used to determine pore size distribution, which is a common method to characterize mesoporous materials.

2.5.2. PZC

PZC of the frameworks materials was determined following the procedure described in a previous study [38]. Assays were done using 20 mg of adsorbent in 10 mL of 0.1 M $NaNO_3$ electrolyte solutions, with pH values between 2 and 12, approximately adjusted using HNO_3 and NaOH aqueous solutions.

Once solutions were prepared, they were kept under magnetic stirring 24 h, giving enough time to achieve charge equilibrium in the adsorbent surface. After that, samples were centrifuged at 4400 rpm for 6 min (Centrifuge Eppendorf 5702) and supernatant pH was measured. Then, the differences between initial and final pH were plotted versus initial pH and the PZC was the pH value on the intersection with X axis.

2.5.3. XRD

XRD analysis was done using X PERT PRO MRD diffractometer (Pananalytical), measuring at an angular range between 20 ° and 80 ° 2ɵ degrees at a scan speed of 0.5°/min. Data were fitted with Cu-Kα radiation ($\lambda = 1.5418$ Å) and analyzed using the Highscore software.

2.5.4. SEM

SEM measurements were done using the JEOL JSM-6700 f coupled to energy dispersive X-Ray spectroscopy (EDS) analysis for element distribution analysis.

2.5.5. XPS

XPS was measured using the Thermo Scientific NEXSA (XPS) instrument equipped with Al Kα monochromatized radiation at 1486.6 eV X-ray source.

2.5.6. FTIR

FTIR was used for investigating the presence of functional groups and the coordination environment. Data was attained using the Vertex 80 V spectrometer (Bruker).

2.5.7. Electrochemical characterization

Electrochemical impedance spectroscopy (EIS) by attaining Nyquist graphs, the measurement of the electrochemical behavior by the realization of cyclic voltammetries (CVs) and the evaluation of the electrochemical active surface area (ECSA) was carried out on the Autolab PGSTAT302N. For that, and following our previous procedures [39,40], Pt was used as the counter electrode, calomel as reference and Ni foam (1 cm^2) was used as working electrode. 0.5 mg of the structured materials were drop-deposited on the working electrode by adding the proper amount of a mixture of 2 mg of the material in 1000 μL EtOH and 50 μL of Nafion. ECSA was calculated by dividing de double layer capacitance (C_{dl}) by the specific capacitance [41] (which is 40 μF cm^{-2} in an atomically smooth planar surface, in alkaline media and with a surface area of 1 cm^2 [42]). C_{dl} was calculated by performing CVs at different scan rates and calculating the current variation between positive and negative currents at a given potential. C_{dl} is half the slope of the straight line attained by the representation of the current difference vs scan rate [41].

2.6. Adsorption evaluation

2.6.1. Adsorption isotherm

For the adsorption isotherms measurements, 36 mg of adsorbent was mixed with 21 mL of a pollutant solution at room temperature for 90 min. Subsequently, the Langmuir, Freundlich, Temkin and Redlich-Peterson models were fitted to the attained data.

Langmuir model (Eq. (2)) is the most used one to describe chemical adsorption processes, assuming adsorbate molecules are retained in active sites across the adsorbent material surface [43].

$$q_e = \frac{q_m K_L C_e}{1 + K_L C_e} \quad (2)$$

Where q_e is the solid amount adsorbed by adsorbent unity at equilibrium (mg g^{-1}); q_m is the maximum pollutant amount adsorbed by adsorbent unity (mg g^{-1}); C_e is the pollutant concentration in the solution at equilibrium (mg L^{-1}) and K_L is Langmuir empirical constant (L mg^{-1}).

Freundlich model (Eq. (3)) is commonly used to represent non-linear adsorption phenomena [43].

$$q_e = K_F C_e^{\frac{1}{n}} \tag{3}$$

Where q_e is the pollutant amount adsorbed by adsorbent unity at equilibrium (mg g^{-1}); C_e is the pollutant concentration in the solution at equilibrium (mg L^{-1}); K_F is an empirical constant that shows adsorption capacity in the solution phase ($L^{1/n}\bullet mg^{1-1/n}\bullet g^{-1}$) and n is a constant (when n = 1, the model is reduced to linearity).

In Temkin model (Eq. (4)) it is assumed that adsorption occurs in different layers and extreme adsorbate concentration values in the liquid phase are considered [44].

$$q_e = \frac{RT}{b}\ln(K_T C_e) \tag{4}$$

Where q_e is the pollutant amount adsorbed by adsorbent unity at equilibrium (mg g^{-1}); C_e is the pollutant concentration in the solution at equilibrium (mg L^{-1}); K_T is an empirical constant (L g^{-1}); R is the ideal gases constant (8314 J $mol^{-1}K^{-1}$); T is the temperature (298 K) and b is another empirical constant (J mol^{-1}).

Redlich-Peterson model (Eq. (5)) is a hybrid model from Langmuir and Freundlich, which is widely applied in homogeneous or heterogeneous adsorption processes [45].

$$q_e = \frac{K_{RP} C_e}{1 + \alpha_{RP} C_e^{\beta}} \tag{5}$$

Where q_e is the pollutant amount adsorbed by adsorbent unity at equilibrium (mg g^{-1}); C_e is the pollutant concentration in the solution at equilibrium (mg L^{-1}); K_{RP} is an empirical constant (L g^{-1}); α_{RP} is another empirical constant (L mg^{-1}) and β is R.P. exponent (with values between 0 and 1).

2.6.2. Adsorption kinetics

For kinetics experiments, 0.18 g of structured adsorbent and 105 mL of the pollutant solution were used. Test samples were taken periodically for analytics during 120 min at room temperature. The collected data was then evaluated using the two most used kinetic models in this area: pseudo-first order and pseudo-second order models.

Pseudo-first order kinetic model (Eq. (6)) tries to explain relations between active sites occupation level along adsorbent surface and empty actives sites [46]. Pseudo-second order kinetic model (Eq. (7)) describes chemisorption processes between the adsorbent and the pollutant [46].

$$Q_t = Q_e(1 - e^{-k_1 t}) \tag{6}$$

$$Q_t = \frac{k_2 Q_e^2 t}{1 + k_2 Q_e t} \tag{7}$$

Where Q_t is the pollutant amount adsorbed by adsorbent unity in a determined time instant t (mg g^{-1}); Q_e is the pollutant amount adsorbed by adsorbent unity at equilibrium (mg g^{-1}); k_1 is empirical pseudo-first order kinetic constant (min^{-1}); k_2 is empirical pseudo-second order kinetic constant (g mg^{-1} min^{-1}); and t represents the time (min).

3. Results

3.1. Characterization of the synthesized adsorbents

The synthesized MIL–53(Al), MIL–53(Al)–F127, NH_2–MIL–101(Fe), and Fe_3O_4 @COF framework materials (Fig. S3) were subjected to detailed characterization.

3.1.1. Textural properties

N_2 adsorption-desorption isotherms obtained presented some differences between the synthesized compounds (Fig. 1). According to IUPAC classification, it would be possible to identify a type III isotherm in Fig. 1.b for MIL-53(Al). This is usually related to multilayer adsorption with weak interactions between adsorbed molecules and adsorbent involved [47]. The other structured materials fitted to the type II isotherm model, which describes well multi-layered mesoporous materials adsorption processes [48]. In addition to this, type H4 hysteresis loops were observed for MIL-53(Al)-F127 and NH_2-MIL-101(Fe) materials (Fig. 1.c,d). This kind of hysteresis is commonly related to the presence of narrow porous [49]. NH_2-MIL-101(Fe) (Fig. 1.d) presented a higher microporous content, which could be related to its lower surface area and lower gas volume adsorbed (Table S2).

MOFs MIL-53(Al) and F127-MIL-53(Al) showed remarkable specific surface area values (Table S2). This is common in MOFs and COFs and it is one of the reasons they are used for adsorption purposes [50]. This is directly related to the obtained uptakes during adsorption experiments, confirming adsorption processes are favored by adsorbents with higher specific surfaces. Moreover, this high surface area also may favor Fenton catalytic activity, where H_2O_2 can reach easily the materials pores [51].

3.1.2. Speciation

Further, PZC was calculated for the synthesized structured materials, being in all cases below 5 (Fig. S4). The initial pH values of the pollutant solutions were 5.6 for BPA and 6.1 for PDN. The speciation of both pollutants is shown in Fig. S5. The results demonstrate that both PDN and BPA would be in neutral form at the working pH whereas the structured materials would be negatively charged, as above the PZC the adsorbent surface is negatively charged [52]. This suggests that adsorption can take place by π-π interactions or hydrogen bond instead of electrostatic unions [14,51,53], and if so, these latter will be induced dipoles. This explains the weaker interaction between some EDCs and MOFs [54].

These π-π interactions can be possible due to the aromatic characteristics of both pollutants and the complex MOF structure which may have π orbitals on the planes [55]. Indeed, BPA adsorption within MOfs had already been explained previously [15], considering it's a molecule prone to this type of interactions due to its high proportion of aromatic rings [55]. The fact that PDN experiences also a high adsorption degree demonstrates that several complex pollutants could be eliminated with these materials thought π-π interactions. This avoids the need of favouring ionic interactions, avoiding the expensive and time-consuming pH control of real inlets.

3.1.3. Phase composition

The powder XRD pattern of the synthesized samples reveal the overall crystalline structure of the phase-pure framework materials (Fig. S6), one of the typical characteristics of MOFs [50]. Hence, the XRD results show the suitability of the mild conditions of the solvothermal synthesis for their synthesis, keeping the expected crystallinity. Most of the relatively shark peaks are found to be in concordance with previous studies [29–31] confirming the successful synthesis of the MOFs and COF. It is important to note that MIL-53(Al) and MIL-53(Al)-F127 showed the same structure and consequently only MIL-53(Al) is shown. Both materials showed the clearest crystalline structure (Fig. S6), with defined peaks and without organic compounds' baseline noise. This may indicate a more ordered structure.

3.1.4. Morphology and chemical composition

Fig. 2 shows typical SEM images of the synthesized materials, which display aggregated particulate appearance. The chemical EDS analysis confirms the presence of the key constituting element in the synthesized MIL–53(Al), MIL–53(Al)–F127, NH_2–MIL–101(Fe), and Fe_3O_4 @COF frameworks. The estimated element compositions of the products are shown in Fig.S7. Positively, it is an abundance of C and O on all the

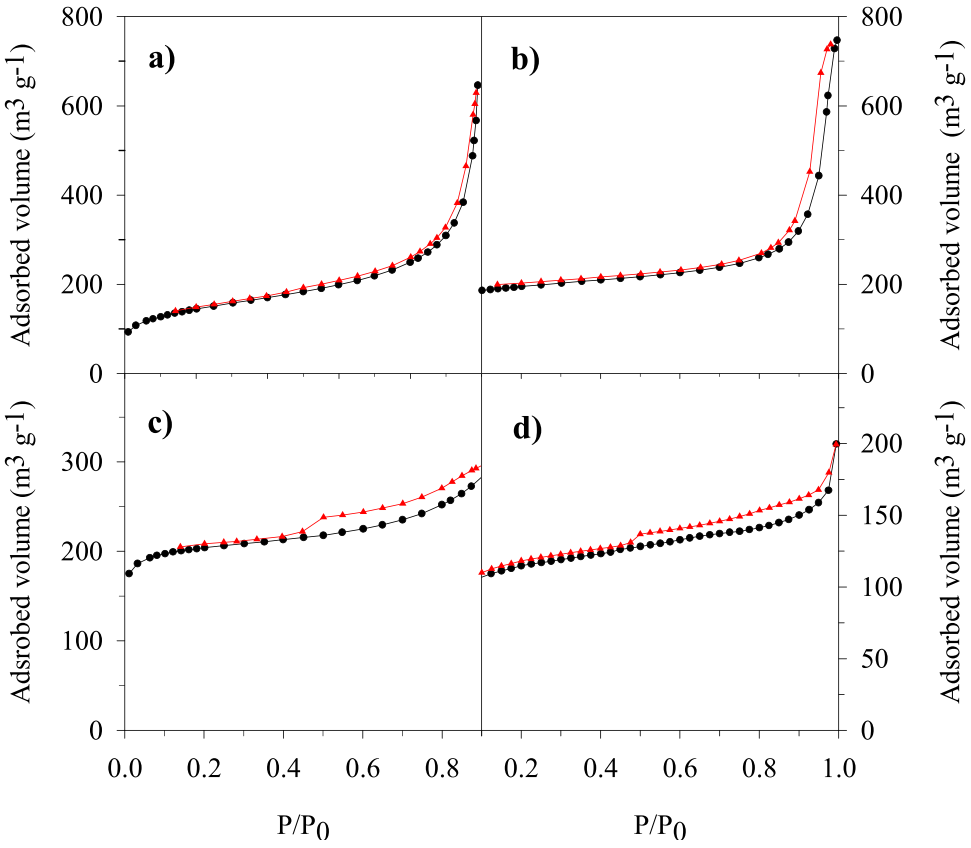

Fig. 1. N_2 adsorption-desorption isotherms for (a) Fe_3O_4 @COF, (b) MIL-53(Al), (c) MIL-53(Al)-F127 and (d) NH_2-MIL-101(Fe).

structured materials, demonstrating the presence of different functional groups which would facilitate electron movement and with that, catalytic performance [56]. Interestingly, the EDS analysis shows that MIL–53(Al) is a carbonaceous structure containing clusters of aluminum oxide (Fig. 2.b). The introduction of the Pluronic F127 during synthesis leads to a formation of smaller aluminum oxide clusters in the MIL–53 (Al)–F127 (Fig. 2.c). In all cases, there is evidence of an homogeneous elemental distribution, which favors adsorption and catalytic behavior [57].

3.1.5. Surface chemical composition

XPS of the synthesized framework compounds was performed. As it can be seen on Fig. 3, survey analysis demonstrates the high content on C and O which may favor adsorption over the functional groups [56]. On the O deconvolution spectra (Fig. S8), it can be detected the presence of -COO and -OH at, respectively, 532.18 and 533.43 eV [15]. Regarding C deconvolution, (Fig. S8), C-C, C═C and C-H bands are detected, reflecting the organic net of the synthesized materials [31]. An increase in O-C═O units in C spectra is observed in MIL-53(Al)-F127 as compared to MIL-53(Al), most likely due to the presence of Pluronic F127. All these double bonds and electronegative compounds favor the van der Waals forces [14,51,54] which are the basis of the interaction between the studied EDCs and these structured organic frameworks (Section 3.1.2).

The metals contained in each structured material are also detected on the survey spectra (Fig. 3). Indeed, Al deconvolution of MIL-53(Al) and MIL-53(Al)-F127 depicts several peaks related to different Al compounds such as Al_2O_3, AlOOH or $AlO_4(OH)_2$ [15] (Fig. S8), which is in concordance with previous EDS results (Fig. 2). On the case of Fe_3O_4 @COF and NH_2-MIL-101(Fe), Fe is in different oxidation states (Fig. S8) which may vary its performance as catalytic-adsorbents [31].

3.1.6. Functional groups

Regarding FTIR results, all the synthesized framework materials show several peaks associated with the containing functional groups (Fig. 4) such as C-OH, C-O-C, C═O, and O-C═O which have been reported to favor adsorption and catalytic activity on structured materials [56]. The samples exhibit peaks between 1700 and 1300 cm^{-1}, which are related to the stretching vibration of the constituting organic ligands [15]. The presence of the benzene molecules in all these structured materials is reflected on the peak at 770 cm^{-1} [31]. The bands observed at 996 cm^{-1} for MIL-MOFs are related to O-H vibration in $AlO_4(OH)_2$ groups [15] demonstrating the successful trapping of Al. Slight differences were detected between MIL-53(Al) and MIL-53(Al)-F127, showing both of them the highest variety of functional groups (Fig. 4). Oppositely, the peak at 1073 cm^{-1} on MIL-53(Al) associated to N-H stretching of unreacted DMF [15] is not detected in MIL-53(Al)-F127, mainly due to the addition of F127 which increases C and O content.

3.1.7. Electrochemical characterization

The untypical catalyst characterization by CVs, EIS and ECSA measurement was done. The suitability of this process for MOFs and COFs characterization was proved by the acquirement of significant differences on the electrochemical behavior of the synthesized structured materials. To begin with, the attained ECSA values (Fig. 5.a) were 6.25, 8.75, 17.5 and 5 cm^{-2} for, respectively Fe_3O_4 @COF, MIL-53(Al), MIL-53(Al)-F127 and NH_2-MIL-101(Fe). These values are in concordance with BET results, demonstrating the metal content on those structured materials makes the available surface area to be electrochemically active. The graphs attained for ECSA calculation can be seen on Fig. S9. CVs (Fig. 9.b) demonstrate a superior performance of NH_2-MIL-101(Fe) as it reaches higher intensities at a given potential, this is related to a faster electron transfer [31].

Nyquist graphs are related to the resistivity of the system [41]. As can be seen on Fig. 5.c, the arc radius increases in the order Fe_3O_4 @COF

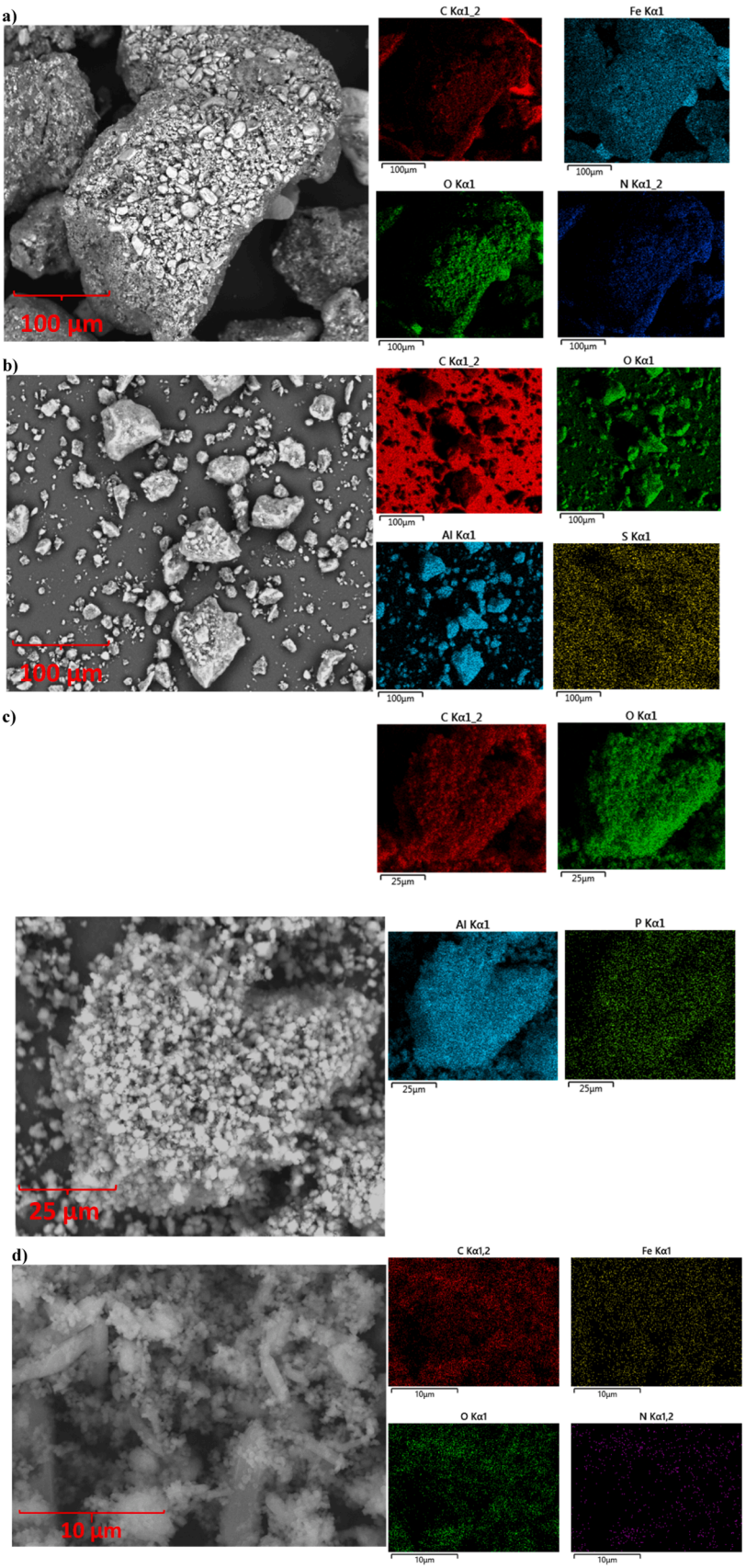

Fig. 2. SEM and EDS distribution for (a) Fe_3O_4 @COF, (b) MIL-53(Al), (c) MIL-53(Al)-F127, and (d) NH_2-MIL-101(Fe).

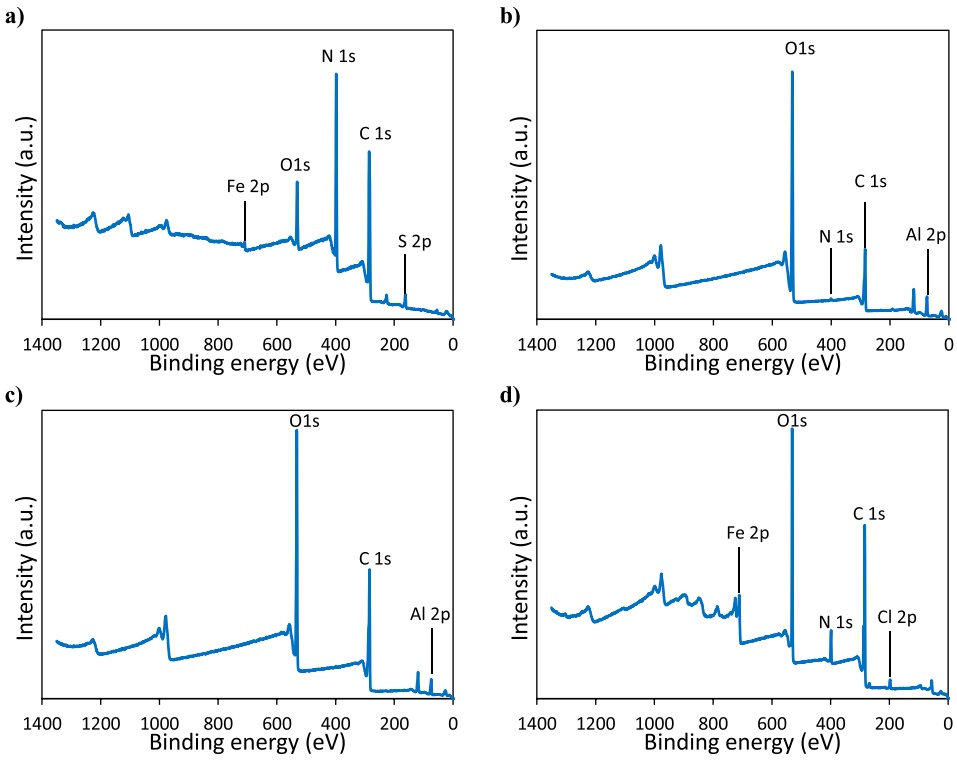

Fig. 3. XPS survey for (a) Fe3O4 @COF, (b) MIL-53(Al), (c) MIL-53(Al)-F127; and (d) NH2-MIL-101(Fe).

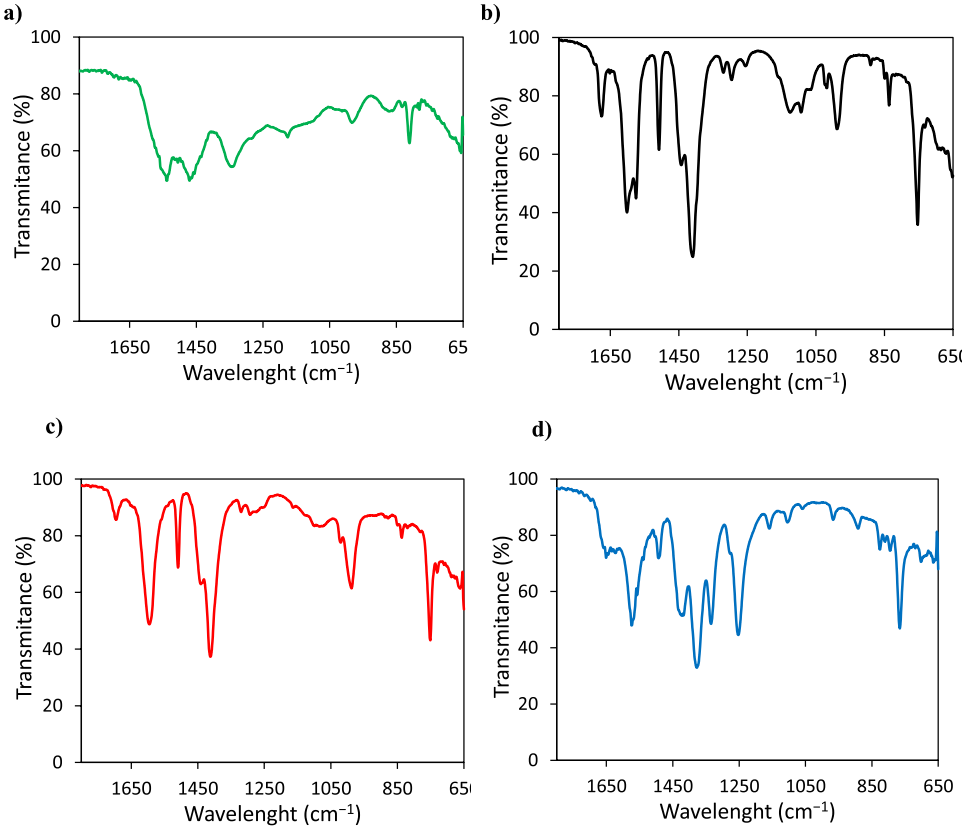

Fig. 4. FTIR spectra for a) Fe_3O_4 @COF, b) MIL-53(Al), c) MIL-53(Al)-F127; d) NH_2-MIL-101(Fe).

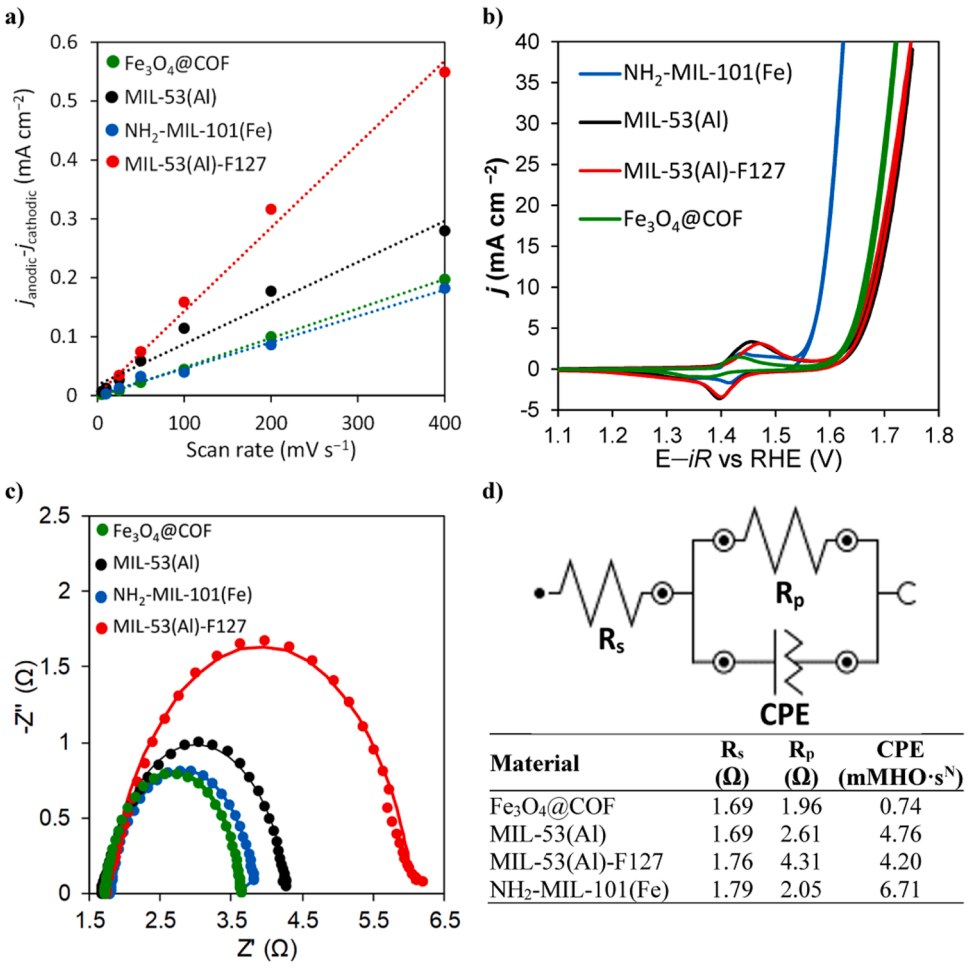

Material	R_s (Ω)	R_p (Ω)	CPE (mMHO·s^N)
Fe_3O_4@COF	1.69	1.96	0.74
MIL-53(Al)	1.69	2.61	4.76
MIL-53(Al)-F127	1.76	4.31	4.20
NH_2-MIL-101(Fe)	1.79	2.05	6.71

Fig. 5. Electrochemical characterization of the structured materials. ECSA calculation (a), CVs (b), Nyquist graphs (c) where the lines represent the equivalent circuit adjustment and equivalent circuit data where R_s and R_p are the series and parallel resistance, respectively and CPE is the Constant Phase Element (d).

< NH_2-MIL-101(Fe) <MIL-53(Al) <MIL-53(Al)-F127, demonstrating the charge separation is less efficient in that order, being more significant on the case of MIL-53(Al)-F127. The other three structured materials have a more elevated electron transfer and thus, they may favor catalytic behavior [31]. Fig. 5.d shows the resistance values attained for the simulated circuit adjustment, it can be seen that R_s, which is related to the electrochemical set-up (electrode and electrolyte) is practically the same in all the structured materials, whereas R_p provides significant

Table 1
Comparison of adsorption capacities before and after regeneration processes of different adsorbents against BPA and PDN.

Adsorbent	Target pollutant	Q (mg g^{-1})	Q_{AR} (mg g^{-1})	Regeneration		Ref.
				Procedure	%	
Fe_3O_4@COF	BPA	168.37	55.53	Fenton-like	32.98	This study
	PDN	27.72	16.14	88 mM H_2O_2	58.23	
MIL-53(Al)	BPA	177.78	148.27		83.40	This study
	PDN	280.70	283.10		100	
MIL-53(Al)-F127	BPA	204.55	26.95		13.18	This study
	PDN	272.30	274.40		100	
NH_2-MIL-101(Fe)	BPA	142.23	38.80		27.28	This study
	PDN	23.92	-		-	
Activated carbon	BPA	56.50	-	-	-	[60]
Porous carbon	BPA	41.8	-	-	-	[60]
C_3N_4-Fe^0	BPA	37.62	n.r.	Photo-Fenton 0.5 mM H_2O_2	75	[27]
Al-MOF-alginate-chitosan	BPA	136.9	131.40	Methanol	96	[15]
MIL-100(Fe)	BPA	55.6	-	-	-	[16]
MOF-74(Zn)-Fe_2O_3	BPA	800	n.r.	PMS/ Pyrolysis	n.r.	[56]
57%TCPP@MOF-808	BPA	94.34	-	-	-	[17]
Citric acid treated hydrochar	PDN	11.37	1.06	Fenton	34.42	[14]
Nanofibers	PDN	174.5	-	-	-	[61]
GO nanoplatelets	PDN	22.94	16.36	NaOH, HCl, NaCl	71.3	[13]
Alginate hydrogel with olive pomace	PDN	3.32	-	-	-	[62]

differences, as it is related to the layer resistance of the material [40]. R_p is much smaller in the structured materials containing Fe, which is in concordance with previous studies [31,41], demonstrating its elevated conductivity attained by its good morphology as well as its higher crystallinity and surface area [41].

3.2. Screening of the adsorbents

The results of the adsorption experiments are summarized in Table 1, where Q is the estimated uptake of either BPA or PDN and Q_{AR} is the uptake after the adsorbent regeneration (in this study, the Fenton-like regeneration after adding 88 mM H_2O_2 for 2 h). In this way, the optimal catalytic adsorbent was selected following the criteria of having maximum BPA and PDN adsorption as well as a high catalytic performance during Fenton-like regeneration.

As it can be seen in Table 1, all the synthesized frameworks exhibit Fenton-like catalytic behavior. This was foreseen by the previous characterization as the structured materials, exhibiting functional groups and metals (Sections 3.1.4–3.1.6) as well as a good electron transfer (Section 3.1.7). Indeed, there are several metals commonly involved in AOPs activation methods, such as Fe [32], Co [58], or Cu [59]. This entails an enhancement compared to traditional adsorption processes, where the spent adsorbent causes a disposal problem. In fact, other authors depicted on Table 1 have adsorbed those EDCs without proposing a regeneration alternative [14,56]. Additionally, other authors have proposed regeneration alternatives usually focused on desorption processes which require the usage of pollutant solutions which change the pollutant from one phase to another, requiring a subsequent treatment [13,15].

On the other hand, other authors have also proposed the catalytic regeneration of spent adsorbents. For instance, Anfruns et al. [34] regenerated activated carbon by the addition of not only H_2O_2 which has innocuous by-products but also Fe^{2+} which possess an environmental problem. Oppositely, in this study, the utilization of those catalytic framework materials facilitates the metal introduction, making possible the Fenton-like regeneration without catalyst addition.

Consequently, even though MIL-53(Al)-F127 provided a 13% higher uptake for BPA adsorption, the fact this catalytic adsorbent lost around 87% of its adsorption capacity after the Fenton-like regeneration, makes MIL-53(Al) the preferred alternative for the cyclic adsorption-regeneration treatment of BPA and PDN. This can be caused by the simpler organic structure of Pluronic F127, which may be degraded during the Fenton-like regeneration, clogging the pores and deteriorating the adsorbent structure and consequently, the following adsorption process. Indeed, some adsorbent modifications based on compounds addition have already reported a reduction on surface area which was attributed to pores clogging [51].

On the other hand, even though Fe_3O_4@COF and NH_2-MIL-101(Fe) also presented a competitive BPA and PDN adsorption, the Fenton-like regeneration was strongly diminished. This can be caused by the fact Fe is not chemically available for the Fenton process to happen. Indeed, Fig. 2 and Fig. S8 demonstrate that Fe is oxidized on both catalytic adsorbents.

Table 1 proves that research has been done for the catalytic-adsorbent usage of MOFs and COFs, although this investigation is on an early stage. Indeed, to our knowledge, PDN had been scarcely studied in terms of elimination and it has never been removed by adsorption with those type of structured materials. Oppositely, other types of adsorbent materials have been essayed for PDN removal, where the attained uptakes are much smaller than those hereby attained with MIL-53(Al). Moreover, the little amount of adsorption processes studies have either not being focused on treating the spent adsorbent or the regeneration step has been carried out mainly by desorption methods [13,15]. There exists a study which also used the Fenton process [14], however, the reached uptake was much smaller than that attained with MIL-53 (Al) and for the regeneration process they required the external addition of 1.53 mM of Fe^{2+}, which makes the regeneration process to be less environmentally friendly.

BPA removal has been already assessed with other MOFs and COFs although in the vast majority of cases the regenerations process was not assessed (Table 1). Some authors have also proposed the usage of MOFs as catalytic materials. Gan et al. [56] reported the activity of MOF-74 (Zn)-Fe_2O_3 on PMS activation. Nevertheless, this process caused damage on the structure and consequently, they opted for a pyrolysis regeneration process. Other studies based the regeneration process on expensive [56] or environmentally un-friendly procedures [15] (Table 1). Only the study reported by Cai et al.[27] used a Fenton-like process for the adsorbent regeneration (in their case C_3N_4 doped with nano zero valent iron) although the high catalytic activity was counteracted by the much smaller uptake attained. This can be caused by the high availability of Fe^0 which was added by impregnation, fact which may clog the pores and impede proper BPA adsorption, favouring iron leaching (0.14 mg/L).

3.3. MIL-53(Al) catalytic adsorbent evaluation

Based on the obtained data, MOF MIL-53(Al) showed decent adsorption capacity for both BPA and PDN as well as an extraordinary catalytic regeneration potential. For these reasons, MIL-53(Al) was selected for the realization of further experiments for the depth evaluation of both the adsorption and regeneration processes.

3.3.1. Isotherms

The adsorption mechanism of both pollutants on MIL-53(Al) was studied. For this reason, the isotherms and kinetic models were evaluated. Initially isotherm models such as Langmuir, Freundlich, Temkin and Redlich-Peterson were fitted to the adsorption data (Fig. 6-A). Among them, Redlich-Peterson model obtained the best fit according to the coefficient of determination (R^2) obtained in both cases (Table S3). This model is common in multilayer adsorption processes where physicochemical interactions are involved [63]. Thus, confirming the Van der Waals forces that were assumed on Section 3.1.2. This model usually adjusts well to homogeneous adsorbents [64], demonstrating the suitable MOF synthesis and corroborating the homogeneity discussed on Section 3.1.4.

Maximum adsorption capacity was 177.78 mg g^{-1} for BPA and 280.70 mg g^{-1} for PDN. BPA uptake is competitive to previously reported data (Table 1), and what is more, this study provides the enhancement of making possible the subsequent Fenton-Like regeneration. On the other hand, to our knowledge, this is the first time a MOF is used for the removal of PDN. Moreover, the uptake attained for PDN removal is higher than that attained with more traditional adsorbents (Table 1).

3.3.2. Kinetic

Both BPA and PDN adsorption was fast (Fig. 6-B) and fitted better to a pseudo-second order kinetic model (Table S4). This is characteristic of adsorption processes where multiple active sites are involved and distributed across the material surface, and with strong chemical interactions between adsorbent and adsorbate [65,66]. This is in concordance with the π- π interactions and/or the hydrogen bonds which may be formed during the adsorption process (Section 3.1.2). In fact, previous authors have noted that pseudo-second order kinetic fitted well PDN adsorption on hydrogels [62] or BPA on MOF-74(Zn)-Fe_2O_3 [56]. This kinetic adjustment demonstrates the adsorption process is deeply related to adsorbate concentration [64].

The quickness of the adsorption process can be noticed in the kinetic constants (Table S4), fact promoted by the rapidity of Van der Waals interactions and the high surface area of the synthesized materials, which favors the adsorbent-adsorbate contact [57]. Indeed, the sorption rate defeated previous adsorbent materials. Flores-Céspedes et al. [67] adsorbed PDN into hydrochar immobilized in alginate-chitosan beads at

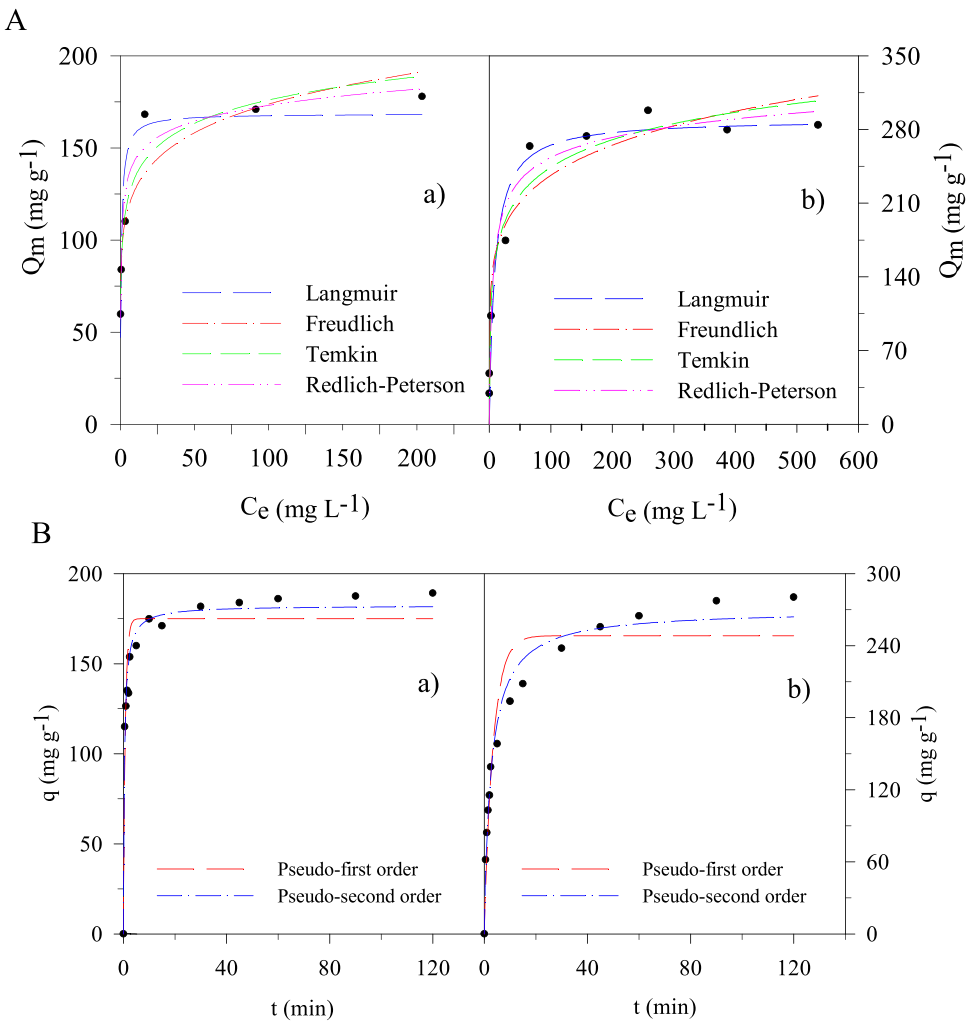

Fig. 6. Adsorption isotherms (A) and kinetics (B) for a) BPA and b) PDN.

a rate of 0.0011 mg g^{-1} min^{-1}, and thus, MIL-53(Al) provides a 18% faster adsorption. Likewise, Gan et al. [56] adsorbed BPA at a pseudo-second order kinetic rate although they required 100 min to achieve equilibrium instead of the 20 min needed in this study. This may be related to the higher porosity [17] of MIL-53(Al) (Section 3.1.1) as well as the presence of a crystalline structure (Section 3.1.3) [30] and functional groups (Sections 3.1.5 and 3.1.6) which may favor π-π interactions [53].

3.4. Real wastewater treatment

With the aim of assessing future usages of this adsorption process, MIL-53(Al) was used for the removal of BPA and PDN from real wastewater (Fig. S10). In this case, adsorption decreased 41% for BPA and 74% for PDN. These are expected results taking into account the higher complexity of the effluent (Table S5). Indeed, Luo et al. [15] reported an uptake decrease of around 60% when having BPA in an effluent with an ionic strength of 0.3 M, due to the higher content of NaCl. This is caused by the competition of Na^+ and BPA (or also PDN in this study) for the active sites of the MOF. Moreover, a higher conductivity causes the interactions between BPA (or PDN) and the adsorbent to be weaker. Indeed, the possibilities of induced dipole electrostatic interactions, which could take place between the neutral BPA and PDN with the negatively charged MOFs, are even more reduced as there exist more ions on the media [54].

Nevertheless, the attained uptakes are competitive to previous research for the treatment of real wastewaters. Indeed, Kebede et al. [61] had an uptake of 154.2 and 113.4 mg g^{-1} of PDN from the effluent and the influent of a real wastewater treatment plant using nanofibers made from *Mondia whitei* root extract.

3.5. MIL-53(Al) reuse

Once MIL-53(Al) is spent with either BPA or PDN, the Fenton-like regeneration took place by the addition of 88 mM H_2O_2. Indeed, catalytic adsorbent reuse is a key feature for future real usages [35]. As can be seen in the graph (Fig. S11), only the first cycle caused a detriment of around 20% on BPA regeneration, then, the adsorbent can be regenerated up to 5 times without detriment. The fact only the regeneration process suffers a detriment on the case of having BPA as pollutant, contrasting the constant PDN regeneration (detriment of 3%) may be due to the polymeric characteristics of BPA which causes clogging to some extent. Nevertheless, 20% is an acceptable detriment and the attained regeneration uptake defeats previous reported results (Table 1). For instance, Bhattacharyya et al. [13] used sodium hydroxide, hydrochloric solution and sodium chloride causing a PDN removal efficiency decrease of 28.7% after 5 cycles. Moreover, other authors may have a lower detriment, but regarding the initial high uptakes of MIL-53 (A), the remaining adsorption performance is higher than previous researchers [13,14,60].

In order to understand the regeneration process, the characterization of the catalytic adsorbent prior and after the regeneration process was

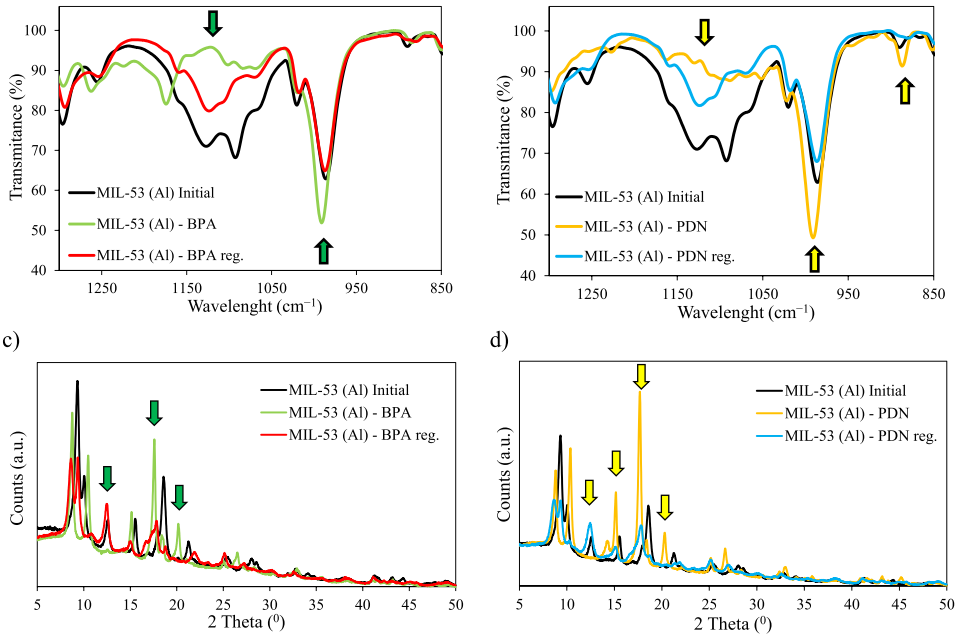

Fig. 7. FTIR (a,b) and XRD (c, spectra prior and after BPA (a,c) or PDN (b,d) adsorption with spectra after Fenton-like regeneration (reg.). The arrows point out the modifications mentioned.

done, in order to confirm its stability in time. Consequently, FTIR and XRD measurements were done. As can be seen in FTIR measurement (Fig. 7.a,b and full spectra on Fig. S12), several differences can be found on the initial, spent and regenerated MIL-53(Al). A significative peak appears at around 996 cm^{-1} on the spent catalytic adsorbent (Fig. 7), demonstrating the presence of C═C due to BPA and PDN addition (also found at 887 cm^{-1} on this latter). This peak recovers its original area after Fenton-like regeneration, demonstrating the structured material is regenerated after the H_2O_2 addition, without losing its main characteristics, which explains it is reusable during 5 cycles (Fig. S11). The small peak at 3665 (Fig. S12) is related to the $AlO_4(OH)_2$ present on this catalytic adsorbent [15]. This peak can be clearly seen on initial and regenerated MIL-53(Al), demonstrating the adsorbent was clogged by either BPA or PDN and that Fenton-like regeneration was successful. The broad peak present between 1050 and 1170 cm^{-1} is related to the catalytic adsorbent structure, as at this wavelength there appears C-N and C═C vibrations which are found within MIL-53(Al) structure. This signal decreases due to the presence of PDN and BPA, due to interactions pollutant-adsorbent [35], and it is recuperated after Fenton-like regeneration (Fig. 7). Similarly, the peak around 3440 cm^{-1} (Fig. S12) which is related to O-H stretching adsorbent [15] which may be related to the organic structure of the MOF and the presence of aluminum hydroxides. This signal is diminished by BPA and PDN addition and it is recovered after MIL-53(Al) regeneration.

In the case of XRD spectra, some additional peaks are found on the polluted MIL-53(Al) which may be caused by some interactions between the catalytic adsorbent and the pollutant. Indeed, Zhao et al. [68] have detected additional peaks at less than 30^0 after the adsorption of a dye in their MOF@SiO_2. The successful regeneration can be confirmed by the similar aspect of both initial and regenerated MIL-53(Al) (Fig S10.c,d) [68].

Hence, the Fenton-like process resulted to degrade softly both BPA and PDN endocrine disruptors, as no significant changes were detected on the regenerated MIL-53(Al) (Fig. S12) and it kept its adsorption capacity during 5 cycles (Fig. S11) This demonstrates the suitability of the Fenton-like process regeneration when compared to previous studies where either the structure was damaged due to regeneration [56] or the functional groups were lost due to too strong interactions MOF-pollutant [35].

In overall, this process could be subsequently studied in order to present a realistic overall treatment alternative. Thus, the quick treatment based on adsorption remediation could be applied for the elimination of EDCs and the powerful AOPs can be used for avoiding adsorbent disposal. Moreover, the usage of adsorption on real wastewaters as a pre-concentration step prior to AOPs makes the application of these latter more efficient, as these processes are suitable for high pollutant concentrations [25,26].

4. Conclusions

The successful synthesis of four structured materials was accomplished. Thus, COF Fe_3O_4 @COF and MOFs MIL-53(Al), MIL-53(Al)-F127 and NH_2-MIL-101(Fe) were attained. They were deeply characterized so their different behavior in terms of both adsorption and regeneration can be explained. In this manner, the characteristics required for a good catalytic-adsorbent are well determined and among them, the high amount of functional groups, a high surface area or the presence of a high ordered structure are highlighted. All of them showed high BPA and PDN adsorption uptakes and capability of being regenerated by Fenton-like process. For the first time a set of novel MOFs and COF have been used for coupling adsorption-AOPs process as a complete remediation alternative. Particularly, MIL-53(Al) adsorption uptakes obtained were 177.78 mg g^{-1} and 280.70 mg g^{-1} for BPA and PDN, respectively. In addition to this, MIL-53(Al) showed the best performance in terms of Fenton-like regeneration (83.14% and 100% for BPA and PDN, respectively), proving aluminum can catalyze Fenton-like reactions. Thus, the adsorption process was studied by the realization of adsorption kinetics and isotherms, as well as by the evaluation of the effect of a real wastewater matrix. This catalytic adsorbent was reused up to 5 times, demonstrating the high stability of MIL-53(Al). These results surpass previously reported data, encompassing both traditional adsorbents and new materials. They demonstrate solid performance not only as an adsorbent but also as a catalyst. Therefore, this study promotes the future utilization of adsorption-regeneration process as a fast but environmentally friendly wastewater treatment alternative. In order to evaluate it applicability in large-scale volumes, reactor design possibilities and energy cost of the whole process should be further investigated.

CRediT authorship contribution statement

Kolenko Yury V.: Funding acquisition, Resources, Supervision, Validation, Writing – review & editing. **Sanroman M. Ángeles:** Conceptualization, Funding acquisition, Investigation, Project administration, Supervision, Validation, Visualization, Writing – review & editing. **Pazos Marta:** Conceptualization, Funding acquisition, Methodology, Project administration, Supervision, Visualization, Writing – review & editing. **Garcia Ocampo Juanjo:** Data curation, Formal analysis, Investigation, Writing – original draft. **Díez Aida M.:** Conceptualization, Data curation, Formal analysis, Investigation, Methodology, Supervision, Validation, Visualization, Writing – original draft.

Declaration of Competing Interest

The authors declare that they have no known competing financial interests or personal relationships that could have appeared to influence the work reported in this paper.

Data availability

Data will be made available on request.

Acknowledgments

This work was supported by MCIN/AEI/10.13039/501100011033 [Project PID2020-113667GBI00]. The researcher Aida M. Díez is grateful to Xunta de Galicia (ED481D-2023/015) and to Deputación Provincial de Pontevedra for the financial support obtained. This work has been funded by MCIN/AEI/10.13039/501100011033 and European Union Next Generation funds EU/PRTR (PDC2021-121394-I00). The researcher Juanjo García-Ocampo is thankful to University of Vigo for the grant (Erasmus+ practices program) which financed the research carried out at INL. Funding for open access charge: Universidade de Vigo/CISUG.

Appendix A. Supporting information

Supplementary data associated with this article can be found in the online version at doi:10.1016/j.jece.2023.111820.

References

[1] A.L. Camargo-Perea, A. Rubio-Clemente, G.A. Peñuela, Use of ultrasound as an advanced oxidation process for the degradation of emerging pollutants in water, Water (Switz.) 12 (2020) 1068–1090, https://doi.org/10.3390/W12041068.
[2] A.I. Stefanakis, J.A. Becker, A review of emerging contaminants in water: classification, sources, and potential risks, in: impact water pollut, Hum. Heal. Environ. Sustain (2015) 55–80, https://doi.org/10.4018/978-1-4666-9559-7.ch003.
[3] J. Michałowicz, Bisphenol a - sources, toxicity and biotransformation, Environ. Toxicol. Pharmacol. 37 (2014) 738–758, https://doi.org/10.1016/j.etap.2014.02.003.
[4] S. Almeida, A. Raposo, M. Almeida-González, C. Carrascosa, Bisphenol A: food exposure and impact on human health, Compr. Rev. Food Sci. Food Saf. 17 (2018) 1447–1639, https://doi.org/10.1111/1541-4337.12388.
[5] P. Kongsted, I.M. Svane, H. Lindberg, G. Daugaard, L. Sengeløv, Low-dose prednisolone in first-line docetaxel for patients with metastatic castration-resistant prostate cancer: Is there a clinical benefit? Urol. Oncol. Semin. Orig. Investig. 33 (2015) 494.e15–494.e20, https://doi.org/10.1016/j.urolonc.2015.06.022.
[6] P.L. McNeil, C. Nebot, A. Cepeda, K.A. Sloman, Environmental concentrations of prednisolone alter visually mediated responses during early life stages of zebrafish (Danio rerio), Environ. Pollut. 218 (2016) 981–987, https://doi.org/10.1016/j.envpol.2016.08.048.
[7] S.W. Lv, J.M. Liu, Z.H. Wang, H. Ma, C.Y. Li, N. Zhao, S. Wang, Recent advances on porous organic frameworks for the adsorptive removal of hazardous materials, J. Environ. Sci. 80 (2019) 169–185, https://doi.org/10.1016/j.jes.2018.12.010.
[8] X. Liu, H. Pang, X. Liu, Q. Li, N. Zhang, L. Mao, M. Qiu, B. Hu, H. Yang, X. Wang, Orderly porous covalent organic frameworks-based materials: superior adsorbents for pollutants removal from aqueous solutions, 100076–100103, Innov 2 (2021), https://doi.org/10.1016/j.xinn.2021.100076.
[9] S.P.S. Fernandes, V. Romero, B. Espiña, L.M. Salonen, Tailoring covalent organic frameworks to capture water contaminants, Chem. A Eur. J. 25 (2019) 6455–6664, https://doi.org/10.1002/chem.201806025.
[10] J.I. Martinez-Costa, R. Leyva-Ramos, E. Padilla-Ortega, Sorption of diclofenac from aqueous solution on an organobentonite and adsorption of cadmium on organobentonite saturated with diclofenac, Clays Clay Min. 66 (2018) 515–528, https://doi.org/10.1346/CCMN.2018.064119.
[11] Y. Song, Q. Sun, B. Aguila, S. Ma, Opportunities of covalent organic frameworks for advanced applications, 1801410–1801443, Adv. Sci. 6 (2019), https://doi.org/10.1002/advs.201801410.
[12] J. Wang, S. Zhuang, Covalent organic frameworks (COFs) for environmental applications, 213046–213061, Coord. Chem. Rev. 400 (2019), https://doi.org/10.1016/j.ccr.2019.213046.
[13] S. Bhattacharyya, P. Banerjee, S. Bhattacharya, R.K.S. Rathour, S.K. Majumder, P. Das, S. Datta, Comparative assessment on the removal of ranitidine and prednisolone present in solution using graphene oxide (GO) nanoplatelets, Desalin. Water Treat. 132 (2018) 287–296, https://doi.org/10.5004/dwt.2018.23170.
[14] B. Hayoun, S. Escudero-Curiel, M. Bourouina, S. Bourouina-Bacha, M. Angeles Sanromán, M. Pazos, Preparation and characterization of high performance hydrochar for efficient adsorption of drugs mixture, 118797–118808, J. Mol. Liq. 353 (2022), https://doi.org/10.1016/j.molliq.2022.118797.
[15] Z. Luo, H. Chen, S. Wu, C. Yang, J. Cheng, Enhanced removal of bisphenol A from aqueous solution by aluminum-based MOF/sodium alginate-chitosan composite beads, 124493–124501, Chemosphere 237 (2019), https://doi.org/10.1016/j.chemosphere.2019.124493.
[16] F.X. Qin, S.Y. Jia, Y. Liu, H.Y. Li, S.H. Wu, Adsorptive removal of bisphenol A from aqueous solution using metal-organic frameworks, Desalin. Water Treat. 54 (2015) 93–102, https://doi.org/10.1080/19443994.2014.883331.
[17] L. Han, X. Liu, X. Zhang, M. Li, D. Li, P. Qin, S. Tian, M. Lu, Z. Cai, Preparation of multivariate zirconia metal-organic frameworks for highly efficient adsorption of endocrine disrupting compounds, J. Hazard. Mater. 424 (2022), https://doi.org/10.1016/j.jhazmat.2021.127559.
[18] U. Qumar, J.Z. Hassan, R.A. Bhatti, A. Raza, G. Nazir, W. Nagban, M. Ikram, Photocatalysis vs adsorption by metal oxide nanoparticle, J. Mater. Sci. Technol. 131 (2022) 122–166, https://doi.org/10.1016/j.jmst.2022.05.020.
[19] I. Ouiriemmi, A.M. Díez, M. Pazos, M.Á. Sanromán, Iron-loaded catalytic silicate adsorbents: synthesis, characterization, electroregeneration and application for continuous removal of 1-butylpyridinium chloride, Catalysts 10 (2020) 950–971, https://doi.org/10.3390/catal10090950.
[20] P. Hu, M. Long, Cobalt-catalyzed sulfate radical-based advanced oxidation: a review on heterogeneous catalysts and applications, Appl. Catal. B Environ. 181 (2016) 103–117, https://doi.org/10.1016/j.apcatb.2015.07.024.
[21] C. Li, W. Peng, Z. Fang, J. Liu, Water pollutants oxidation degradation through the activation of peroxymonosulfate (PMS) heterogeneously catalyzed by transition metal oxide: a review, Cailiao Daobao Mater. Rev. 32 (2018) 2223–2229, https://doi.org/10.11896/j.issn.1005-023X.2018.13.013.
[22] M. Cheng, G. Zeng, D. Huang, C. Lai, P. Xu, C. Zhang, Y. Liu, Hydroxyl radicals based advanced oxidation processes (AOPs) for remediation of soils contaminated with organic compounds: a review, Chem. Eng. J. 284 (2016) 582–598, https://doi.org/10.1016/j.cej.2015.09.001.
[23] Y. Deng, R. Zhao, Advanced oxidation processes (AOPs) in wastewater treatment, Curr. Pollut. Rep. 1 (2015) 167–176, https://doi.org/10.1007/s40726-015-0015-z.
[24] A.G. Capodaglio, Critical perspective on advanced treatment processes for water and wastewater: AOPs, ARPs, and AORPs, Appl. Sci. 10 (2020) 4549–4575, https://doi.org/10.3390/app10134549.
[25] S. Sabatino, A. Galia, O. Scialdone, Electrochemical abatement of organic pollutants in continuous-reaction systems through the assembly of microfluidic cells in series, ChemElectroChem 3 (2016), https://doi.org/10.1002/celc.201500409.
[26] G. Donoso, J.R. Dominguez, T. González, S. Correia, E.M. Cuerda-Correa, Electrochemical and sonochemical advanced oxidation processes applied to tartrazine removal. Influence of operational conditions and aqueous matrix, 111517–111529, Environ. Res. 202 (2021), https://doi.org/10.1016/j.envres.2021.111517.
[27] M. Cai, J. Li, F. Wu, G. Voyard, G. Mailhot, M. Brigante, Synergistic degradation of bisphenol A in heterogeneous Fenton and photo-Fenton systems catalyzed by graphitized carbon-nano zero valent iron, 110959–110967, J. Environ. Chem. Eng. 11 (2023), https://doi.org/10.1016/j.jece.2023.110959.
[28] A.M. Díez, M. Pazos, M.A. Sanromán, Synthesis of magnetic-photo-Fenton catalyst for degradation of emerging pollutant, Catal. Today 328 (2019) 267–273, https://doi.org/10.1016/j.cattod.2018.12.042.
[29] L. You, K. Xu, G. Ding, X. Shi, J. Li, S. Wang, J. Wang, Facile synthesis of Fe3O4@COF covalent organic frameworks for the adsorption of bisphenols from aqueous solution, 114456–114465, J. Mol. Liq. 320 (2020), https://doi.org/10.1016/j.molliq.2020.114456.
[30] M. Zhou, Y. nan Wu, J. Qiao, J. Zhang, A. McDonald, G. Li, F. Li, The removal of bisphenol A from aqueous solutions by MIL-53(Al) and mesostructured MIL-53(Al), J. Colloid Interface Sci. 405 (2013) 157–163, https://doi.org/10.1016/j.jcis.2013.05.024.
[31] X. Li, W. Guo, Z. Liu, R. Wang, H. Liu, Quinone-modified NH2-MIL-101(Fe) composite as a redox mediator for improved degradation of bisphenol A, J. Hazard. Mater. 324 (2017) 665–672, https://doi.org/10.1016/j.jhazmat.2016.11.040.
[32] A.M. Díez, M.A. Sanromán, M. Pazos, Fenton-based processes for the regeneration of catalytic adsorbents, Catal. Today 313 (2018) 122–127, https://doi.org/10.1016/j.cattod.2017.10.030.

[33] J.T. Mourand, J.C. Crittenden, D.W. Hand, D.L. Perram, S. Notthakun, Regeneration of spent adsorbents using homogeneous advanced oxidation, Water Environ. Res. 67 (1995) 355–363, https://doi.org/10.2175/106143095×131583.
[34] A. Anfruns, M.A. Montes-Morán, R. Gonzalez-Olmos, M.J. Martin, H2O2-based oxidation processes for the regeneration of activated carbons saturated with volatile organic compounds of different polarity, Chemosphere 91 (2013) 48–54, https://doi.org/10.1016/j.chemosphere.2012.11.068.
[35] A.A. Taha, L. Huang, S. Ramakrishna, Y. Liu, MOF [NH2-MIL-101(Fe)] as a powerful and reusable Fenton-like catalyst, 101004–101013, J. Water Process Eng. 33 (2020), https://doi.org/10.1016/j.jwpe.2019.101004.
[36] A.M. Díez, F.C. Moreira, B.A. Marinho, J.C.A. Espíndola, L.O. Paulista, M. A. Sanromán, M. Pazos, R.A.R. Boaventura, V.J.P. Vilar, A step forward in heterogeneous photocatalysis: Process intensification by using a static mixer as catalyst support, Chem. Eng. J. 343 (2018) 597–606, https://doi.org/10.1016/j.cej.2018.03.041.
[37] F. Ambroz, T.J. Macdonald, V. Martis, I.P. Parkin, Evaluation of the BET theory for the characterization of meso and microporous MOFs, 1800173–1800189, Small Methods 2 (2018), https://doi.org/10.1002/smtd.201800173.
[38] J.S. Noh, J.A. Schwarz, Estimation of the point of zero charge of simple oxides by mass titration, J. Colloid Interface Sci. 130 (1989) 157–164, https://doi.org/10.1016/0021-9797(89)90086-6.
[39] A.M. Díez, M. Pazos, M.Á. Sanromán, Y.V. Kolen'ko, GO-TiO2 as a Highly Performant Photocatalyst Maximized by Proper Parameters Selection, Int. J. Environ. Res. Public Health 19 (2022) 11874–11887, https://doi.org/10.3390/ijerph191911874.
[40] A.M. Díez, I. Núñez, M. Pazos, M.Á. Sanromán, Y.V. Kolen'ko, Fluoride-Doped TiO2 photocatalyst with enhanced activity for stable pollutant degradation, Catalysts 12 (2022) 1190–1208, https://doi.org/10.3390/catal12101190.
[41] B. Shabbir, M.Z. Ansari, S. Manzoor, A.G. Abid, M.N. Ashiq, T.A. Taha, Facile synthesis of Er-MOF/Fe2O3 nanocomposite for oxygen evolution reaction, 126861–126869, Mater. Chem. Phys. 292 (2022), https://doi.org/10.1016/j.matchemphys.2022.126861.
[42] T. Kang, J. Kim, Optimal cobalt-based catalyst containing high-ratio of oxygen vacancy synthesized from metal-organic-framework (MOF) for oxygen evolution reaction (OER) enhancement, 150035–150043, Appl. Surf. Sci. 560 (2021), https://doi.org/10.1016/j.apsusc.2021.150035.
[43] A. Balouch, M. Kolachi, F.N. Talpur, H. Khan, M.I. Bhanger, Sorption kinetics, isotherm and thermodynamic modeling of defluoridation of ground water using natural adsorbents, Am. J. Anal. Chem. 04 (2013) 221–228, https://doi.org/10.4236/ajac.2013.45028.
[44] L. Chiao, R.G. Rinker, A kinetic study of ammonia synthesis: modeling high-pressure steady-state and forced-cycling behavior, Chem. Eng. Sci. 44 (1989) 9–19, https://doi.org/10.1016/0009-2509(89)85227-3.
[45] O. Redlich, D.L. Peterson, A useful adsorption isotherm, J. Phys. Chem. 63 (1959) 1024, https://doi.org/10.1021/j150576a611.
[46] U.A. Edet, A.O. Ifelebuegu, Kinetics, isotherms, and thermodynamic modeling of the adsorption of phosphates from model wastewater using recycled brick waste, Processes 8 (2020) 665–680, https://doi.org/10.3390/PR8060665.
[47] A. Aqel, Using of nanomaterials to enhance the separation efficiency of monolithic columns, Nanomater. Chromatogr. Curr. Trends Chromatogr. Res. Technol. Tech. (2018) 299–322, https://doi.org/10.1016/B978-0-12-812792-6.00010-8.
[48] M.A. Al-Ghouti, D.A. Da'ana, Guidelines for the use and interpretation of adsorption isotherm models: a review, 122383–122405, J. Hazard. Mater. 393 (2020), https://doi.org/10.1016/j.jhazmat.2020.122383.
[49] M. Eddaoudi, Characterization of porous solids and powders: surface area, pore size and density By S. Lowell (Quantachrome Instruments, Boynton Beach), J. E. Shields (C. W. Post Campus of Long Island University), M. A. Thomas, and M. Thommes (Quantachrome In-struments, J. Am. Chem. Soc. 127 (2005) 14117–14120, https://doi.org/10.1021/ja041016i.
[50] K.A. Adegoke, O.R. Adegoke, R.A. Adigun, N.W. Maxakato, Two-dimensional metal-organic frameworks: from synthesis to biomedical, environmental, and energy conversion applications, 214817–214874, Coord. Chem. Rev. 473 (2022), https://doi.org/10.1016/j.ccr.2022.214817.
[51] M. Minale, Z. Gu, A. Guadie, D.M. Kabtamu, Y. Li, X. Wang, Application of graphene-based materials for removal of tetracyclines using adsorption and photocatalytic-degradation: a review, 111310–111328, J. Environ. Manag. 276 (2020), https://doi.org/10.1016/j.jenvman.2020.111310.
[52] D.D. Medina, J.M. Rotter, Y. Hu, M. Dogru, V. Werner, F. Auras, J.T. Markiewicz, P. Knochel, T. Bein, Room temperature synthesis of covalent-organic framework films through vapor-assisted conversion, J. Am. Chem. Soc. 137 (2015) 1016–1019, https://doi.org/10.1021/ja510895m.
[53] N. Cheng, B. Wang, P. Wu, X. Lee, Y. Xing, M. Chen, B. Gao, Adsorption of emerging contaminants from water and wastewater by modified biochar: a review, 116448–116462, Environ. Pollut. 273 (2021), https://doi.org/10.1016/j.envpol.2021.116448.
[54] F. Hooriabad Saboor, N. Nasirpour, S. Shahsavari, H. Kazemian, The effectiveness of MOFs for the removal of pharmaceuticals from aquatic environments: a review focused on antibiotics removal, Chem. Asian J. 17 (2022), https://doi.org/10.1002/asia.202101105.
[55] H. Li, C. Lin, R. Ma, Y. Chen, π–π stack driven competitive /complementary adsorption of aromatic compounds on MIL-53(Al), 139377–139384, Chemosphere 337 (2023), https://doi.org/10.1016/j.chemosphere.2023.139377.
[56] L. Gan, L. Wang, L. Xu, X. Fang, C. Pei, Y. Wu, H. Lu, S. Han, J. Cui, J. Shi, C. Mei, Fe3C-porous carbon derived from Fe2O3 loaded MOF-74(Zn) for the removal of high concentration BPA: The integrations of adsorptive/catalytic synergies and radical/non-radical mechanisms, J. Hazard. Mater. 413 (2021) 125305–125320. https://doi.org/10.1016/j.jhazmat.2021.125305.
[57] Y. Yang, Y. Gu, H. Lin, B. Jie, Z. Zheng, X. Zhang, Bicarbonate-enhanced iron-based Prussian blue analogs catalyze the Fenton-like degradation of p-nitrophenol, J. Colloid Interface Sci. 608 (2022) 2884–2895, https://doi.org/10.1016/j.jcis.2021.11.015.
[58] J. Hou, X. He, S. Zhang, J. Yu, M. Feng, X. Li, Recent advances in cobalt-activated sulfate radical-based advanced oxidation processes for water remediation: a review, 145311–145325, Sci. Total Environ. 770 (2021), https://doi.org/10.1016/j.scitotenv.2021.145311.
[59] J. Pan, B. Gao, P. Duan, K. Guo, X. Xu, Q. Yue, Recycling exhausted magnetic biochar with adsorbed Cu2+ as a cost-effective permonosulfate activator for norfloxacin degradation: Cu contribution and mechanism, 125413–125424, J. Hazard. Mater. 413 (2021), https://doi.org/10.1016/j.jhazmat.2021.125413.
[60] T. Asada, K. Oikawa, K. Kawata, S. Ishihara, T. Iyobe, A. Yamada, Study of removal effect of bisphenol A and β-estradiol by porous carbon, J. Heal. Sci. 50 (2004) 588–593, https://doi.org/10.1248/jhs.50.588.
[61] T.G. Kebede, M.B. Seroto, R.C. Chokwe, S. Dube, M.M. Nindi, Adsorption of antiretroviral (ARVs) and related drugs from environmental wastewaters using nanofibers, 104049–104058, J. Environ. Chem. Eng. 8 (2020), https://doi.org/10.1016/j.jece.2020.104049.
[62] F. Flores-Céspedes, M. Villafranca-Sánchez, M. Fernández-Pérez, Alginate-based hydrogels modified with olive pomace and lignin to removal organic pollutants from aqueous solutions, Int. J. Biol. Macromol. 153 (2020) 883–891, https://doi.org/10.1016/j.ijbiomac.2020.03.081.
[63] N. Ayawei, A.N. Ebelegi, D. Wankasi, Modelling and interpretation of adsorption isotherms, J. Chem. 2017 (2017) 1–11, https://doi.org/10.1155/2017/3039817.
[64] W. Hao, T.M. Vadas, J.R. McCutcheon, Chemically activated carbon nanofibers for adsorptive removal of bisphenol-A: batch adsorption and breakthrough curve study, Chin. J. Chem. Eng. 61 (2023) 248–259, https://doi.org/10.1016/j.cjche.2023.03.017.
[65] H.K. Agbovi, L.D. Wilson, Adsorption processes in biopolymer systems: fundamentals to practical applications, Nat. Polym. Green. Adsorbents Water Treat. (2021) 1–51, https://doi.org/10.1016/b978-0-12-820541-9.00011-9.
[66] Y.S. Ho, G. McKay, Kinetic models for the sorption of dye from aqueous solution by wood, Process Saf. Environ. Prot. 76 (1998) 183–191, https://doi.org/10.1205/095758298529326.
[67] C. Li, Z. Xiong, J. Zhang, C. Wu, The strengthening role of the amino group in metal-organic framework MIL-53 (Al) for methylene blue and malachite green dye adsorption, J. Chem. Eng. Data. 60 (2015) 3414–3422, https://doi.org/10.1021/acs.jced.5b00692.
[68] R. Zhao, H. Liao, X. Wu, X. Cao, Selective adsorption behaviours of MOFs@SiO2 with different pore sizes and shell thicknesses, 121693–121703, J. Solid State Chem. 292 (2020), https://doi.org/10.1016/j.jssc.2020.121693.